European Congress on Computational Methods in Applied Sciences and Engineering
ECCOMAS 2004
P. Neittaanmäki, T. Rossi, S. Korotov, E. Oñate, J. Périaux, and D. Knörzer (eds.)
Jyväskylä, 24–28 July 2004

CBS STABILIZATION IN DYNAMICS OF SOLIDS USING EXPLICIT TIME INTEGRATION

Jerzy Rojek*, **Eugenio Oñate**†, **and Robert L. Taylor**‡

Paper dedicated to Professor O.C. Zienkiewicz

*Institute of Fundamental Technological Research
Polish Academy of Sciences
ul. Swietokrzyska 21, 00-049 Warsaw, Poland
e-mail: jrojek@ippt.gov.pl

† International Center for Numerical Methods in Engineering (CIMNE)
Universitat Politécnica de Catalunya (UPC), Gran Capitán, s/n, Barcelona, Spain
e-mails: onate@cimne.upc.es

Department of Civil and Environmental Engineering
University of California, Berkeley, USA
rlt@ce.berkeley.edu

Key words: CBS, volumetric locking, stabilization, dynamic analysis, explicit time integration.

Abstract. *The characteristic based split (CBS) stabilization procedure developed originally in fluid mechanics has been adapted successfully to solid mechanics problems. The CBS algorithm has been implemented within a finite element program using an explicit time integration scheme. Volumetric locking of linear triangular and tetrahedral elements has been successfully eliminated. The performance of the numerical algorithm is illustrated with numerical results. Comparisons with an alternative stabilization technique based on the Finite Calculus method also are given.*

1 INTRODUCTION

Many finite elements exhibit so called "volumetric locking" in the analysis of incompressible or quasi-incompressible problems in fluid and solid mechanics. Situations of this type are usual in the structural analysis of rubber materials, some geomechanical problems and most bulk metal forming processes. Volumetric locking is an undesirable effect leading to incorrect numerical results [1].

Volumetric locking in solids is present in all low order elements based on the standard displacement formulation. The use of a mixed formulation or a selective integration technique eliminates the volumetric locking in many elements. These methods however, fail in some elements such as linear triangles and tetrahedra, due to lack of satisfaction of the Babuška-Brezzi conditions [1, 2, 3] or alternatively the mixed patch test [1, 4, 5] not being passed. Most linear triangular and tetrahedral elements developed within a mixed formulation also suffer volumetric locking. This poses serious limitations on the possibilities of finite element simulation of processes involving large elasto-plastic deformations like metal forming processes. Even nowadays there is hardly any meshing program that can discretize complex three dimensional geometrical shapes of formed parts avoiding tetrahedral elements. Special stabilizing techniques must be developed to eliminate volumetric locking in linear triangles and tetrahedra.

Considerable efforts have been made in recent years to develop linear triangles and tetrahedra producing correct (stable) results under incompressible situations. Brezzi and Pitkäranta [6] proposed to extend the equation for the volumetric strain rate constraint for Stokes flows by adding a laplacian of pressure term. A similar method was derived for quasi-incompressible solids by Zienkiewicz and Taylor [1]. Other methods to overcome volumetric locking are based on mixed displacement (or velocity)-pressure formulations using the Galerkin-Least-Square (GLS) method [7], average nodal pressure and average nodal deformation techniques [8, 9], and Sub-Grid Scale (SGS) methods [10, 11, 12] and the approach based on the finite calculus (FIC) formulation [13].

The characteristc based split (CBS) stabilization method has been developed in fluid dynamics [14, 15]. Zienkiewicz *et al.* [16] have extended this technique to solid mechanics within explicit dynamic finite element formulation. This algorithm has been further developed to consider bulk metal forming problems [17].

In this paper application of the CBS algorithm in solid mechanics will be reviewed. Basic continuum and discretized finite element equations are given. The constitutive model describing large elasto-plastic deformations of metals is presented. Finally a summary of an alternative stabilization algorithm based on the Finite Calculus (FIC) is given [13].

Several numerical examples illustrating the performance of the CBS algorithm with linear triangles and tetrahedra are presented. Numerical examples range from 2D and 3D analysis of an impact problem to bulk forming problems. Numerical results obtained using the CBS method are compared with the results obtained with the FIC algorithm and with solutions using hexahedral elements based on a mixed formulation.

2 THE CHARACTERISTIC BASED SPLIT ALGORITHM FOR SOLIDS

2.1 Continuous equations

The characteristic based split algorithm for solids has been derived in [16]. The algorithm obtained in fluid mechanics has been extended to solid mechanics by introducing an appropriate constitutive model for a solid material in split equations describing the solid material deformation. Here the derivation of the CBS algorithm for solids will be briefly reviewed.

The problem is governed by the Stokes equations. Large elasto-plastic deformations are considered with a small amount of compressibility allowed, as this generally is the case with large deformation behavior of solids.

The equations expressing the momentum conservation are written as follows

$$\begin{aligned} \rho\,\frac{\partial v_i}{\partial t} &= \frac{\partial s_{ij}}{\partial x_j} + \frac{\partial p}{\partial x_i} + b_i \\ \frac{\partial u_i}{\partial t} &= v_i \end{aligned} \tag{1}$$

where ρ is the density, v_i the velocity in the i direction, s_{ij} the deviatoric stress component, p the mean stress (or pressure), b_i the i component of body force and u_i the displacement in the i-direction. Equations of motion (1) are completed with appropriate boundary conditions and constitutive equations for deviatoric part of stresses s_{ij} and pressure p. The elasto-plastic constitutive model with $J2$ plasticity is presented later on. The constitutive law for pressure is as follows

$$\frac{1}{K}\frac{\partial p}{\partial t} = \frac{\partial v_i}{\partial x_i} \tag{2}$$

where K is the bulk modulus of the material. The boundary conditions prescribe velocities

$$v_i = \hat{v}_i \quad \text{on } \Gamma_v \tag{3a}$$

and tractions

$$t_i = \hat{t}_i = n_j(\hat{s}_{ij} - \delta_{ij}\ \hat{p}) \quad \text{on } \Gamma_t \ . \tag{3b}$$

Application of a standard, Galerkin, finite element discretization of displacement $\mathbf{u}$, velocity $\mathbf{v}$ and pressure p

$$\begin{aligned} \mathbf{u} &\approx \tilde{\mathbf{u}} = \mathbf{N}_v\ \bar{\mathbf{u}} \\ \mathbf{v} &\approx \tilde{\mathbf{v}} = \mathbf{N}_v\ \bar{\mathbf{v}} \\ p &\approx \tilde{p} = \mathbf{N}_p\ \bar{\mathbf{p}}(t) \end{aligned} \tag{4}$$

to Eqs. (1) and (2), gives the discrete equations of mixed formulation, cf. [1]

$$\begin{aligned}\mathbf{M}\frac{\mathrm{d}}{\mathrm{d}t}\bar{\mathbf{v}} &= \mathbf{R}_v - \mathbf{f}_d - \mathbf{C}\bar{\mathbf{p}} \\ \frac{\mathrm{d}\bar{\mathbf{u}}}{\mathrm{d}t} &= \bar{\mathbf{v}} \\ \mathbf{M}_p\frac{\mathrm{d}\bar{\mathbf{p}}}{\mathrm{d}t} &= \mathbf{R}_p + \mathbf{C}^T\bar{\mathbf{v}} \quad .\end{aligned} \tag{5}$$

In the above $\bar{\mathbf{v}}$ and $\bar{\mathbf{p}}$ stand for the sets of unknown nodal parameters, the matrices are given by, cf. [1]

$$\begin{aligned}\mathbf{M} &= \rho\int_\Omega \mathbf{N}_v^T\mathbf{N}_v\,\mathrm{d}\Omega\,, \qquad \mathbf{M}_p = \frac{1}{K}\int_\Omega \mathbf{N}_p^T\mathbf{N}_p\,\mathrm{d}\Omega \\ \mathbf{R}_v &= \int_{\Gamma_t}\mathbf{N}_v^T\hat{\mathbf{t}}\;\mathrm{d}\Gamma + \int_\Omega \mathbf{N}_v^T\mathbf{b}\,\mathrm{d}\Omega\,, \qquad \mathbf{R}_p = \mathbf{0} \\ \mathbf{f}_d &= \int_\Omega \mathbf{B}_v^T\mathbf{s}\,\mathrm{d}\Omega\,, \qquad \mathbf{C} = \int_\Omega \mathbf{N}_v^T\boldsymbol{\nabla}\mathbf{N}_p\,\mathrm{d}\Omega\end{aligned} \tag{6}$$

where $\mathbf{B}$ is the linear stress–strain operator matrix, stress deviator $\mathbf{s}$ can be determined assuming arbitrary (isotropic) constitutive model.

With a fully incompressible material $\mathbf{M}_p$ would be zero and this would not permit the application of time step procedures of the explicit type. Small compressibility allows us to adopt fully explicit solution scheme. In the explicit solution the two matrices $\mathbf{M}$ and $\mathbf{M}_p$ are usually diagonalized.

The standard mixed formulation performs well for certain combinations of velocity and pressure discretization, which lead to finite elements satisfying Babuška–Brezzi stability conditions, like quadrilaterals and hexahedra with linear displacement(velocity) and constant pressure interpolations. Elements not satisfying Babuška–Brezzi conditions, for instance linear triangles and tetrahedra with equal order velocity and pressure interpolation, suffer volumetric locking.

This difficulty can be overcome by the use of operator splitting procedures (or fractional step methods).

2.2 The fractional step method

In the fractional step method the equations are split into parts. The sum of the parts, however, must be such that the original equations are always recovered. The split can be applied to discretized equations, cf. [18]. Here we will follow a "classical" procedure [14, 15], where the split is applied to the equations of the continuum (1) and (2) following their time discretization using the trapezoidal rule (or θ method). After temporal discretization the equations have the following form

$$\rho\,\frac{v_i^{n+1}-v_i^n}{\Delta t}=\frac{\partial s_{ij}}{\partial x_j}^{n}+\frac{\partial p}{\partial x_i}^{n+\theta_2}+b_i^n$$
$$\frac{u_i^{n+1}-u_i^n}{\Delta t}=v_i^{n+\theta_3} \qquad (7a)$$

and

$$\frac{1}{K}\frac{p^{n+1}-p^n}{\Delta t}=\frac{\partial v_i^{n+\theta_1}}{\partial x_i} \qquad (7b)$$

where $\Delta t=t^{n+1}-t^n$, n and $n+1$ are consecutive time instants, and θ_J are generalized mid-point rule discretization parameters. Note that the deviatoric stress and body force terms in Eq. (7a) are evaluated at different temporal points than the pressure. This is to facilitate the split introduced next. For an arbitrary variable ϕ we have the following relationship

$$\phi^{n+\theta_j}=(1-\theta_j)\phi^n+\theta_j\phi^{n+1} \qquad (8)$$

with $0\le\theta_j\le 1$. In our case θ_1 can vary between 0.5 and 1, while θ_2 and θ_3 can vary between 0 and 1. In all that follows we shall use $\theta_1=1$.

The momentum equation (7a) is rewritten in the following form

$$\rho\,\frac{v_i^{n+1}-v_i^*+v_i^*-v_i^n}{\Delta t}=\frac{\partial p^{n+\theta_2}}{\partial x_i}+\frac{\partial s_{ij}^n}{\partial x_j}+b_i^n \qquad (9)$$

and split into two equations:

$$\rho\,\frac{v_i^*-v_i^n}{\Delta t}=\frac{\partial s_{ij}^n}{\partial x_j}+b_i^n \qquad (10a)$$

$$\rho\,\frac{v_i^{n+1}-v_i^*}{\Delta t}=\frac{\partial p^{n+\theta_2}}{\partial x_i} \qquad (10b)$$

where the fictitious velocity v_i^* is called the fractional velocity. The fractional velocity is obtained from Eq. (10a)

$$v_i^*=v_i^n+\frac{\Delta t}{\rho}\frac{\partial s_{ij}^n}{\partial x_j}+\Delta t b_i^n \qquad (11a)$$

and the real velocity is calculated from Eq. (10b) as

$$v_i^{n+1}=v_i^*+\frac{\Delta t}{\rho}\frac{\partial p^{n+\theta_2}}{\partial x_j}\quad . \qquad (11b)$$

Substituting Eq. (11b) into Eq. (7b)

$$\frac{1}{K}\frac{p^{n+1}-p^n}{\Delta t}=\frac{\partial v_i^*}{\partial x_i}+\frac{\Delta t}{\rho}\frac{\partial^2 p^{n+\theta_2}}{\partial x_i^2}\quad . \qquad (11c)$$

Finally, from the second of Eq. (7a) we obtain

$$u_i^{n+1} = u_i^n + \Delta t v_i^{n+\theta_3} \quad . \tag{11d}$$

The CBS algorithm stated above consists of the following four steps:

(i) Calculate the fractional velocity v_i^* from Eq. (11a);

(ii) Calculate the pressure p^{n+1} from Eq. (11c);

(iii) Calculate the real velocity v_i^{n+1} from Eq. (11b);

(iv) Calculate the displacement u_i^{n+1} from Eq. (11d).

2.3 Finite element discretization

Introducing the finite element space discretization of pressure and velocities given by Eq. (4) and applying the Galerkin method to Eqs. (11a), (11c) and (11b) leads to the following set of discrete equations:

$$\begin{aligned}
\mathbf{M}\frac{\Delta\bar{\mathbf{v}}^*}{\Delta t} &= \mathbf{R}_v - \mathbf{f}_d \\
\frac{1}{\Delta t}\,\mathbf{M}_p\left(\bar{\mathbf{p}}^{n+1} - \bar{\mathbf{p}}^n\right) &= -\,\mathbf{C}^T\,\bar{\mathbf{v}}^n + \tilde{\mathbf{C}}\,\Delta\bar{\mathbf{v}}^\star - \Delta t\,\mathbf{H}\,\bar{\mathbf{p}}^{n+\theta_2} - \mathbf{R}_p \\
\mathbf{M}\frac{\bar{\mathbf{v}}^{n+1} - \bar{\mathbf{v}}^*}{\Delta t} &= -\mathbf{C}\bar{\mathbf{p}}^{n+\theta_2} \\
\bar{\mathbf{u}}^{n+1} &= \bar{\mathbf{u}}^n + \Delta t\bar{\mathbf{v}}^{n+\theta_3}
\end{aligned} \tag{12}$$

where the additional new matrices are defined as follows

$$\begin{aligned}
\Delta\bar{\mathbf{v}}^\star &= \bar{\mathbf{v}}^* - \bar{\mathbf{v}}^n \\
\tilde{\mathbf{C}} &= \int_\Omega (\nabla\cdot\mathbf{N}_p)^T\,\mathbf{N}_v\,\mathrm{d}\Omega \\
\mathbf{H} &= \int_\Omega \nabla\mathbf{N}_p^T\frac{1}{\rho_0}\nabla\mathbf{N}_p\,\mathrm{d}\Omega \\
\mathbf{R}_v &= \int_{\Gamma-\Gamma_t}\mathbf{N}_v\mathbf{s}\,\mathrm{d}\Gamma + \int_{\Gamma_t}\mathbf{N}_v(\hat{\mathbf{t}} - \mathbf{n}p)\,\mathrm{d}\Gamma + \int_\Omega \mathbf{N}_v^T\mathbf{b}\,\mathrm{d}\Omega \\
\mathbf{R}_p &= \int_{\Gamma_v}\mathbf{N}_p^T\,\mathbf{n}^{\mathrm{T}}\bar{\mathbf{v}}\,\mathrm{d}\Gamma \quad .
\end{aligned} \tag{13}$$

Evaluation of the second integral in $\mathbf{R}_v$ requires the "extraction" of the pressure part from the prescribed traction on the part of the boundary Γ_t. This can be done taking the pressure from the previous time step as an estimation. A similar estimation must be made for the deviatoric stresses $\mathbf{s}$ on the part of the boundary $\Gamma - \Gamma_t$ to calculate the first integral in $\mathbf{R}_v$. In a simplified algorithm these troublesome calculations are avoided and the vectors $\mathbf{R}_v$ and $\mathbf{R}_p$ are evaluated according to the second of Eq. (6). This simplification implies the non-physical boundary condition

$$\frac{\partial p}{\partial n} = 0 \quad \text{on } \Gamma \tag{14}$$

and introduces a certain error in the pressure. It can be demonstrated, however, that this error is localized to narrow boundary areas, cf. [19]. This simplification is employed in the numerical algorithm presented below. Using this form of the algorithm one avoids computation of $\tilde{\mathbf{C}}$, as well as, avoids integrations of the projections of deviatoric stresses on the velocity boundaries, cf. [16].

2.4 Solution algorithm

(i) Approximate velocity increment determination

$$\Delta \mathbf{v}^{\star} = \Delta t \ \mathbf{M}^{-1} \left(\mathbf{R}_v^n - \mathbf{f}_d^n \right) \tag{15a}$$

(ii) The pressure increment evaluation

$$\left(\frac{1}{\Delta t} \ \mathbf{M}_p + \theta_2 \Delta t \mathbf{H} \right) \Delta \bar{\mathbf{p}} = -\mathbf{C}^T \bar{\mathbf{v}}^{\star} - \Delta t \ \mathbf{H} \ \bar{\mathbf{p}}^n \tag{15b}$$

(iii) The velocity correction

$$\Delta \bar{\mathbf{v}} = \Delta \bar{\mathbf{v}}^{\star} - \Delta t \ \mathbf{M}^{-1} \mathbf{C} \bar{\mathbf{p}}^{n+1} \tag{15c}$$

(iv) The displacement update

$$\bar{\mathbf{u}}^{n+1} = \bar{\mathbf{u}}^n + \Delta t \bar{\mathbf{v}}^{n+\theta_3} \quad . \tag{15d}$$

The algorithm presented can be used either in a semi-implicit form with an implicit solution of the pressure equation (15b) or in a fully explicit manner taking $\theta_2 = 0$. This paper presents results obtained with a fully explicit algorithm.

2.5 Elasto-plastic constitutive model

The constitutive model used in any analysis of metal forming process must properly represent complex deformation and elasto-plastic properties of the material. The elasto-plastic constitutive model used in our analysis is that presented in [20]. In the description of large elasto-plastic deformations the multiplicative decomposition of the deformation gradient tensor $\mathbf{F}$ into its elastic $\mathbf{F}^{\mathrm{e}}$ and plastic part $\mathbf{F}^{\mathrm{p}}$ is assumed

$$\mathbf{F} = \mathbf{F}^{\mathrm{e}} \mathbf{F}^{\mathrm{p}} \quad . \tag{16}$$

The model is developed in a stress-free intermediate configuration, and then all the constitutive relationships are transformed to the deformed configuration.

In the deformed configuration the following additive decomposition of the Almansi strain tensor $\mathbf{e}$ into the elastic and plastic parts, $\mathbf{e}^{\mathrm{e}}$ and $\mathbf{e}^{\mathrm{p}}$, respectively, is obtained:

$$\mathbf{e} = \mathbf{e}^{\mathrm{e}} + \mathbf{e}^{\mathrm{p}} \quad . \tag{17}$$

The Almansi strain tensor, and its elastic and plastic parts, $\mathbf{e}$, $\mathbf{e}^{\mathrm{e}}$ and $\mathbf{e}^{\mathrm{p}}$, can be expressed by the deformation gradient tensor $\mathbf{F}$ and its elastic part $\mathbf{F}^{\mathrm{e}}$ and plastic part $\mathbf{F}^{\mathrm{p}}$ in the following form:

$$\begin{aligned} \mathbf{e}^{\mathrm{e}} &= \tfrac{1}{2}(\mathbf{I} - \mathbf{F}^{\mathrm{e}-\mathrm{T}}\,\mathbf{F}^{\mathrm{e}-1})\,, \\ \mathbf{e}^{\mathrm{p}} &= \tfrac{1}{2}(\mathbf{F}^{\mathrm{e}-\mathrm{T}}\,\mathbf{F}^{\mathrm{e}-1} - \mathbf{F}^{-\mathrm{T}}\,\mathbf{F}^{-1})\,, \\ \mathbf{e} &= \tfrac{1}{2}(\mathbf{I} - \mathbf{F}^{-\mathrm{T}}\,\mathbf{F}^{-1}) \quad . \end{aligned} \tag{18}$$

The implementation of the general model has been simplified by the assumption that elastic strains are small, which for metals is fully justified. This allows us to assume a simple form of the elastic part of the free energy function ψ^{e}

$$\psi^{\mathrm{e}}(\mathbf{e}^{\mathrm{e}}) = \lambda\,\mathrm{tr}(\mathbf{e}^{\mathrm{e}})^2 \;+\; \mu\,(\mathbf{e}^{\mathrm{e}} : \mathbf{e}^{\mathrm{e}}) \tag{19}$$

where λ and μ are the Lamé constants. With this form of the elastic potential the Kirchhoff stress tensor $\boldsymbol{\sigma}$ is obtained as:

$$\boldsymbol{\sigma} = \frac{\partial \psi^{e}(\mathbf{e}^{\mathrm{e}})}{\partial \mathbf{e}^{\mathrm{e}}} = \lambda\;\mathrm{tr}(\mathbf{e}^{\mathrm{e}}) \;+\; 2\mu\;\mathbf{e}^{\mathrm{e}} \quad . \tag{20}$$

In the present implementation of the model the associated flow rule is assumed with the Huber–Mises yield criterion. The stress–strain curve is taken in the following form

$$\sigma_Y = K(a + \bar{\varepsilon}^{\mathrm{p}})^n \tag{21}$$

where σ_Y is the yield stress and K, a and n are the material constants.

3 STABILIZATION BASED ON FINITE CALCULUS

The finite calculus (FIC) approach has been successfully used to derive stabilized finite element and meshless methods for a wide range of advective-diffusive and fluid flow problems [21, 22]. The same ideas were applied in [13] to derive a stabilized formulation for quasi-incompressible and incompressible solids allowing the use of linear triangles and tetrahedra.

The basis of the FIC method is the satisfaction of the standard equations for balance of momentum (equilibrium of forces) and mass conservation in a domain of finite size and retaining higher order terms in the Taylor expansions used to express the different terms of the differential equations over the balance domain. The modified differential equations contain additional terms which introduce the necessary stability in the equations to overcome the volumetric locking problem.

3.1 Equations of motion

Within the framework of a finite calculus formulation the equations of motion for a solid material are written as, cf. [13]

$$r_i - \frac{h_k}{2}\frac{\partial r_i}{\partial x_k} = 0 \quad \text{in } \Omega \qquad k = 1, n_d \tag{22}$$

where n_d is the number of space dimensions of the problems (i.e. $n_d = 3$ for 3D) and

$$r_i := -\rho\,\frac{\partial^2 u_i}{\partial t^2} + \frac{\partial \sigma_{ij}}{\partial x_j} + b_i \quad . \tag{23}$$

In Eq. (23) ρ is density, t is time, σ_{ij} are stresses, b_i are body forces, and h_k are characteristic length distances of an arbitrary prismatic domain where equilibrium of forces is considered. Equations (22) and (23) are completed with adequate boundary conditions and constitutive equations.

Employing a standard split of stresses into deviatoric and volumetric (pressure) parts, s_{ij} and p, respectively

$$\sigma_{ij} = s_{ij} + p\,\delta_{ij} \tag{24}$$

the governing FIC equations of the mixed displacement-pressure formulation can be obtained in the following form [13]

$$-\rho\,\frac{\Delta v_i}{\Delta t} + \frac{\partial s_{ij}}{\partial x_j} + \frac{\partial p}{\partial x_i} + b_i - \frac{h_k}{2}\frac{\partial r_i}{\partial x_k} = 0 \qquad ; \qquad \frac{\Delta u_i}{\Delta t} - v_i^{n+1/2} = 0 \tag{25a}$$

$$\frac{\Delta p}{K} - \frac{\partial(\Delta u_i)}{\partial x_i} - \sum_{i=1}^{n_d} \tau_i \frac{\partial r_i}{\partial x_i} = 0 \tag{25b}$$

where K is the bulk modulus, ε_v is the volumetric strain and τ_i are *intrinsic time* parameters given by

$$\tau_i = \frac{3h_i^2}{8\,G} \quad . \tag{26}$$

with G being the shear modulus. It can be noted that the value of τ_i deduced from the FIC formulation resembles for $h_i = h_j = h$ that of $\tau = h^2/2G$ heuristically chosen in other works [7].

3.2 Weighted residual forms

The residual r_i is split now as

$$r_i = \pi_i + \frac{\partial p}{\partial x_i} \tag{27}$$

where

$$\pi_i = -\rho\,\frac{\partial v_i}{\partial t} + \frac{\partial s_{ij}}{\partial x_i} + b_i \quad . \tag{28}$$

Note that π_i is the part of r_i not containing the pressure gradient and may be considered as the negative of a projection of the pressure gradient. In a discrete setting the terms π_i can be considered belonging to a space orthogonal to that of the pressure gradient terms. This is similar the stabilization procedure based on a Sub-Grid Scale (SGS) method suggested in [10, 11, 12].

Finally, the weighted residual form of the governing equations is written in the form

$$\int_\Omega \delta u_i \rho \frac{\partial v_i}{\partial t}\,\mathrm{d}\Omega + \int_\Omega \delta\varepsilon_{ij}\sigma_{ij}\,\mathrm{d}\Omega - \int_\Omega \delta u_i b_i\,\mathrm{d}\Omega - \int_{\Gamma_t} \delta u_i \bar{t}_i\,\mathrm{d}\Gamma_t = 0 \tag{29a}$$

$$\int_\Omega \delta v_i \left[\frac{\partial u_i}{\partial t} - v_i\right]\mathrm{d}\Omega = 0 \tag{29b}$$

$$\int_\Omega q\left(\frac{\Delta p}{K} - \frac{\partial(\Delta u_i)}{\partial x_i}\right)\mathrm{d}\Omega + \int_\Omega \left[\sum_{i=1}^{n_d} \frac{\partial q}{\partial x_i}\tau_i\left(\frac{\partial p}{\partial x_i} + \pi_i\right)\right]\mathrm{d}\Omega = 0 \tag{29c}$$

$$\int_\Omega \left[\sum_{i=1}^{n_d} w_i\tau_i\left(\frac{\partial p}{\partial x_i} + \pi_i\right)\right]\mathrm{d}\Omega = 0 \quad . \tag{29d}$$

The stabilization of the momentum equation is necessary in convection dominated problems, this is not relevant for solid mechanics problems, so the additional terms involving the space derivatives of the characteristic lengths have been omitted in Eq. (29a). On the contrary the stabilization term given by the last integral is essential in Eq. (29c).

4 Finite element discretization

Introduction of finite element discretization of the displacements, the pressure and the pressure gradient projection gives the following system of discretized equations

$$\mathbf{M}\frac{\mathrm{d}}{\mathrm{d}t}\bar{\mathbf{v}} - \mathbf{R}_v + \mathbf{f}_d = \mathbf{0} \tag{30a}$$

$$\frac{\mathrm{d}}{\mathrm{d}t}\bar{\mathbf{u}} - \bar{\mathbf{v}} = \mathbf{0} \tag{30b}$$

$$\mathbf{C}^T\Delta\bar{\mathbf{u}} - \mathbf{M}_p\Delta\bar{\mathbf{p}} - \mathbf{L}\bar{\mathbf{p}} - \mathbf{Q}\bar{\boldsymbol{\pi}} = \mathbf{0} \tag{30c}$$

$$\mathbf{Q}^T\bar{\mathbf{p}} + \bar{\mathbf{G}}\bar{\boldsymbol{\pi}} = \mathbf{0} \tag{30d}$$

where the element contributions are given by

$$\begin{aligned}
\mathbf{M} &= \int_\Omega \rho\,\mathbf{N}^T\mathbf{N}\,\mathrm{d}\Omega\,, \qquad \mathbf{C} = \int_\Omega (\nabla\mathbf{N})^T\mathbf{N}\,\mathrm{d}\Omega \\
\mathbf{L} &= \int_\Omega (\nabla\mathbf{N})^T\boldsymbol{\tau}\,\nabla\mathbf{N}\,\mathrm{d}\Omega\,, \quad \mathbf{M}_p = \int_\Omega \frac{1}{K}\mathbf{N}^T\mathbf{N}\,\mathrm{d}\Omega \\
\bar{\mathbf{G}} &= \int_\Omega \mathbf{N}^T\boldsymbol{\tau}\mathbf{N}\,\mathrm{d}\Omega\,, \quad \mathbf{Q} = \int_\Omega (\nabla\mathbf{N})^T\boldsymbol{\tau}\,\mathbf{N}\mathrm{d}\Omega \\
\mathbf{R}_v &= \int_\Omega \mathbf{N}\,\mathbf{b}\,\mathrm{d}\Omega + \int_\Gamma \mathbf{N}\,\bar{\mathbf{t}}\,\mathrm{d}\Gamma\,, \quad \mathbf{f}_d = \int_\Omega \mathbf{B}^T\boldsymbol{\sigma}\,\mathrm{d}\Omega
\end{aligned} \tag{31}$$

and

$$\boldsymbol{\tau} = \begin{bmatrix} \tau_1 & 0 & 0 \\ 0 & \tau_2 & 0 \\ 0 & 0 & \tau_3 \end{bmatrix} \tag{32}$$

The consistent definition of the characteristic length parameters is still an open question. In advective-diffusive and fluid flow problems it is usual to accept that the characteristic length vector has the direction of the velocity vector (this is the so called streamline upwind Petrov-Galerkin or SUPG assumption [23]). In the examples presented in this paper we have obtained good results using a simpler definition of the characteristic lengths with $h_i = h_j = h_{\min}$, where $h_{\min}$ is the smallest of the element (triangles or tetrahedra) heights.

5 Solution scheme

A four step semi-implicit time integration algorithm can be derived from Eqs. (30a)–(30d) as follows:
(i) Compute the nodal velocities $\bar{\mathbf{v}}^{n+1/2}$

$$\bar{\mathbf{v}}^{n+1/2} = \bar{\mathbf{v}}^{n-1/2} + \Delta t\, \mathbf{M}^{-1}(\mathbf{R}_v^n - \mathbf{f}_d^n) \tag{33a}$$

(ii) Compute the nodal displacements $\bar{\mathbf{u}}^{n+1}$

$$\bar{\mathbf{u}}^{n+1} = \bar{\mathbf{u}}^n + \Delta t\, \bar{\mathbf{v}}^{n+1/2} \tag{33b}$$

(iii) Compute the nodal pressures $\bar{\mathbf{p}}^{n+1}$

$$\bar{\mathbf{p}}^{n+1} = [\mathbf{M}_p + \mathbf{L}]^{-1}[\Delta t\, \mathbf{C}^T \bar{\mathbf{v}}^{n+1/2} + \mathbf{M}_p \bar{\mathbf{p}}^n - \mathbf{Q}\bar{\boldsymbol{\pi}}^n] \quad . \tag{33c}$$

(iv) Compute the nodal projected pressure gradients $\bar{\boldsymbol{\pi}}^{n+1}$

$$\bar{\boldsymbol{\pi}}^{n+1} = -\bar{\mathbf{G}}^{-1}\mathbf{Q}^T \bar{\mathbf{p}}^{n+1} \quad . \tag{33d}$$

In above matrices $\mathbf{M}, \mathbf{M}_p, \mathbf{L}, \mathbf{C}, \mathbf{Q}$ and $\bar{\mathbf{G}}$ are evaluated at t^{n+1} and

$$\mathbf{f}_d^n = \int_\Omega [\mathbf{B}^T \boldsymbol{\sigma}]^n \, \mathrm{d}\Omega \tag{34}$$

where the stresses $\boldsymbol{\sigma}^n$ are obtained by consistent integration of the adequate (non linear) constitutive law.

Note that steps (i), (ii) and (iv) are fully explicit. A fully explicit algorithm can be obtained by computing $\bar{\mathbf{p}}^{n+1}$ from step (iii) in Eq. (33c) as follows

$$\bar{\mathbf{p}}^{n+1} = \mathbf{M}_p^{-1}[\Delta t\, \mathbf{C}^T \bar{\mathbf{v}}^{n+1/2} + (\mathbf{M}_p + \mathbf{L})\bar{\mathbf{p}}^n - \mathbf{Q}\boldsymbol{\pi}^n] \quad . \tag{35}$$

Obviously, the explicit solution is efficient if diagonal forms of matrices $\mathbf{M}_p$, $\mathbf{M}$ and $\bar{\mathbf{G}}$ are used.

6 NUMERICAL RESULTS

6.1 Impact of a cylindrical bar

The problem analysed is the impact of a cylindrical bar with initial velocity of 227 m/s into a rigid wall. The bar has an initial length 32.4 mm and initial radius 3.2 mm. Material properties of the bar are typical of copper: density $\rho = 8930$ kg/m^3, Young's modulus $E = 1.17 \cdot 10^5$ MPa, Poisson's ratio $\nu = 0.35$, initial yield stress $\sigma_Y = 400$ MPa and hardening modulus $H = 100$ MPa. A time period of 80 μs has been analyzed.

Figure 1 shows 2D and 3D solutions using triangular and tetrahedral elements based on equal order interpolation for displacement and pressure – both solutions exhibit volumetric locking. Figure 2 shows correct numerical solution obtained using quadrilateral elements a mixed displacement-pressure formulation with constant discontinuous pressure in each element. This solution is used as a reference of comparison for the stabilized solution using triangular and tetrahedral elements and the CBS algorithm. The CBS results are also compared to the results obtained using the alternative stabilized algorithm based on finite calculus (FIC). Figures 3 and 4 show results obtained using triangular elements with the CBS algorithm. We can see that the volumetric locking is eliminated, and the distribution and values of the pressure and effective plastic strain are consistent with those obtained using quadrilateral elements as shown in Fig. 2. The two cases have different time steps, taken as 0.6 and 0.15 of the critical time step, respectively. Influence of the time step has been studied. Figure 5 shows the results obtained with triangular elements with the FIC stabilization, with τ taken as $\alpha h^2/G$ with $\alpha = 0.01$. 3D solutions obtained using tetrahedra with the CBS and FIC stabilizations are shown in Figs. 6 and 7, respectively.

Different solutions have been compared in Fig. 8a and 8b which show the pressure variation along the axis of symmetry and along the generatrix, respectively. Although the pressures generally agree there is some divergence especially at the end of the axis of symmetry (Fig. 8a), which could indicate that a certain error is introduced by the approximate treatment of the traction boundary conditions in the simplified split algorithm.

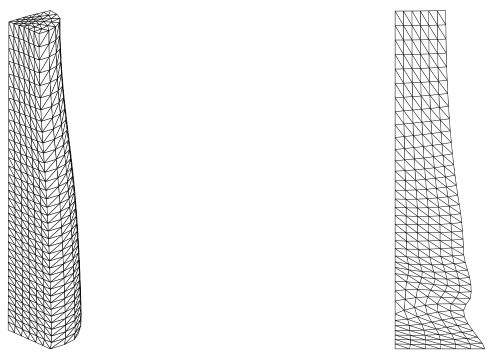

a) b)

Figure 1: Final deformed mesh for standard displacement solution with locking a) 2D solution using axisymmetric triangular elements, b) 3D solutions using tetrahedra elements

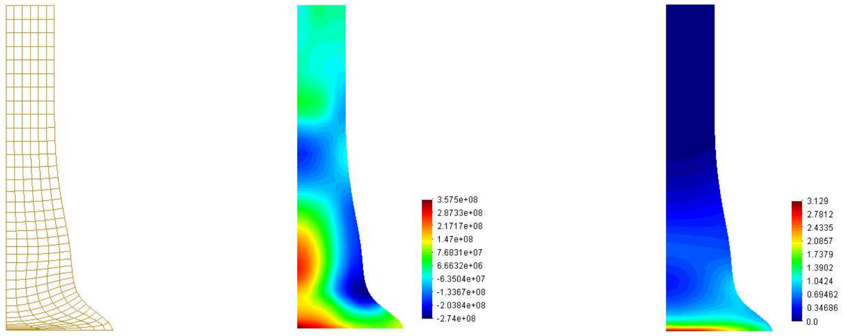

a) b) c)

Figure 2: 2D explicit solution using mixed formulation with quadrilateral elements a) deformed mesh, b) pressure distribution, c) effective plastic distribution

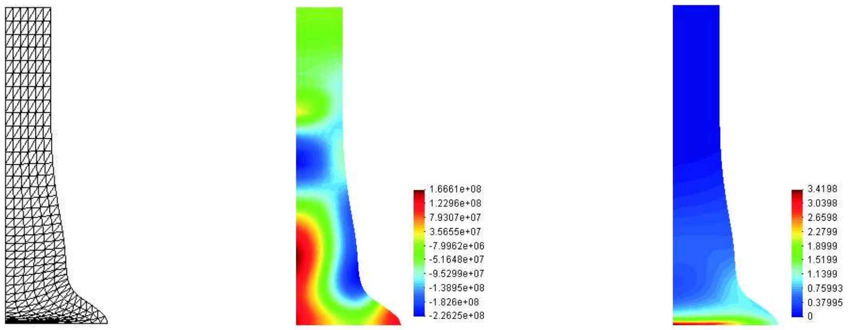

a) b) c)

Figure 3: 2D solution using the CBS algorithm ($\Delta t = 0.60 \Delta t_{\mathrm{cr}}$) a) deformed mesh, b) pressure distribution, c) effective plastic distribution

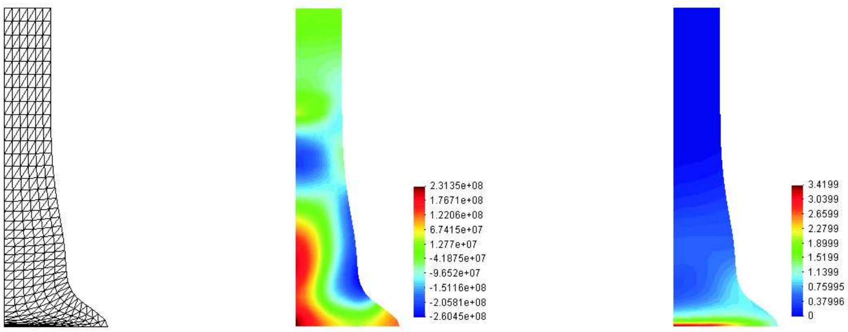

a) b) c)

Figure 4: 2D solution using the CBS algorithm ($\Delta t = 0.15 \Delta t_{\mathrm{cr}}$) a) deformed mesh, b) pressure distribution, c) effective plastic distribution

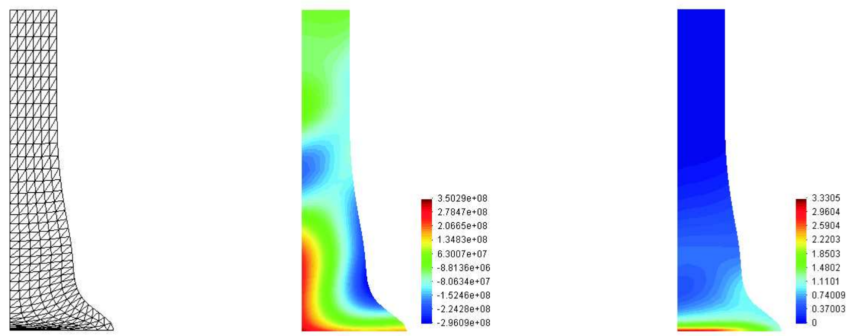

a) b) c)

Figure 5: 2D solution using the FIC formulation ($\alpha = 0.01$) a) deformed mesh, b) pressure distribution, c) effective plastic distribution

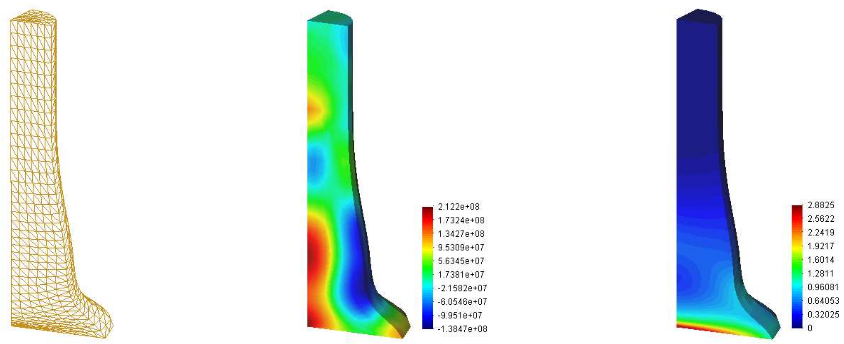

a) b) c)

Figure 6: 3D using the CBS formulation a) deformed mesh, b) pressure distribution, c) effective plastic distribution

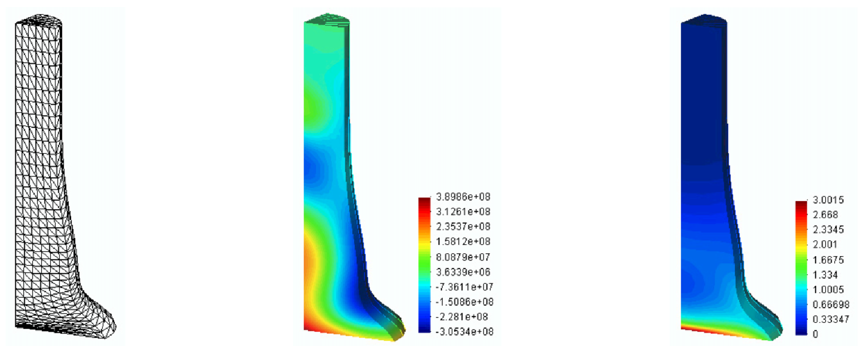

a) b) c)

Figure 7: 3D solution using the FIC formulation ($\alpha = 0.01$) a) deformed mesh, b) pressure distribution, c) effective plastic distribution

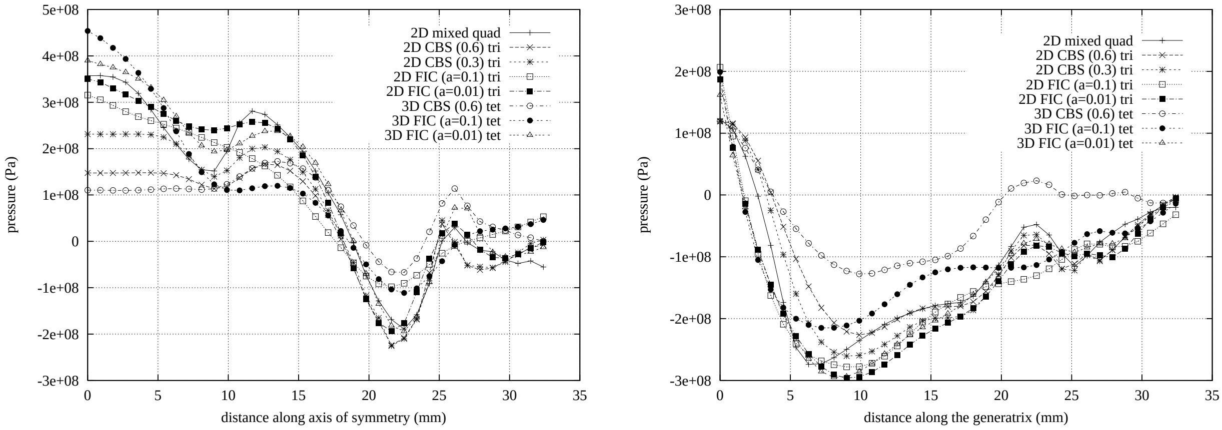

Figure 8: Pressure distribution in different solutions: a) along the axis of symmetry, b) along the generatrix

6.2 Sidepressing of a cylinder

A cylinder 100 mm long with a radius of 100 mm is subjected to sidepressing between two plane dies. It is compressed to 100 mm. The material properties are the following: $E = 217$ GPa, $\nu = 0.3$, $\rho = 7830$ kg/m^3, $\sigma_0 = 170$ MPa, $H = 30$ MPa, friction coefficient $= 0.2$. The die velocity is assumed to be 2 m/s. Initial set-up is shown in Figure 9. A quarter of a cylinder was discretized with hexahedra or tetrahedra.

Figure 10 shows the results obtained using hexahedral mesh and mixed formulation. The results are shown in the form of deformed shape with distribution of the effective plastic strain and pressure. These results will be treated as the reference ones for other solutions. Figure 11 and 12 show the results obtained using the CBS algorithm for two different meshes of tetrahedra. The results obtained with the FIC stabilization are shown in Fig. 13. Quite a good agreement can be seen between different solutions presented. The agreement is confirmed in Fig. 14b, which presents the variation of the pressure along the line $ABCDEA$ defined in Fig. 14a.

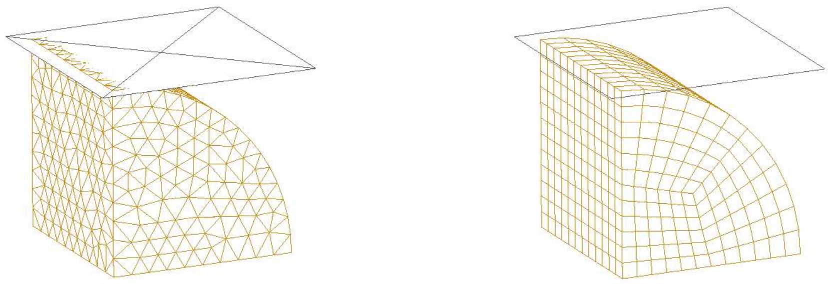

Figure 9: Sidepressing of a cylinder: (a) initial tetrahedral mesh; (b) initial hexahedral mesh

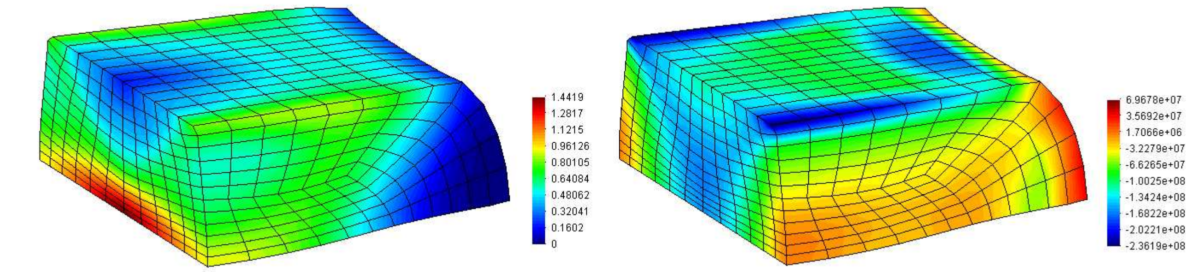

a) b)

Figure 10: Sidepressing of a cylinder, mixed formulation, hexahedral mesh: (a) effective plastic strain; (b) pressure distribution

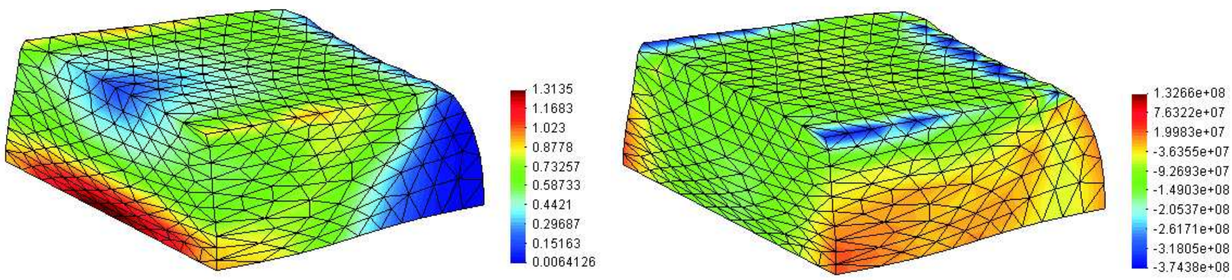

a) b)

Figure 11: Sidepressing of a cylinder, CBS algorithm, tetrahedra, coarse mesh (4090 elements): (a) effective plastic strain; (b) pressure distribution

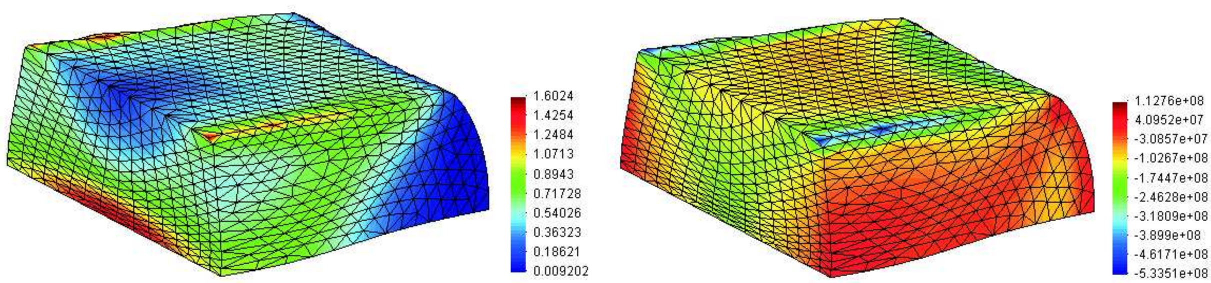

a) b)

Figure 12: Sidepressing of a cylinder, CBS algorithm, tetrahedra, fine mesh (22186 elements): (a) effective plastic strain; (b) pressure distribution

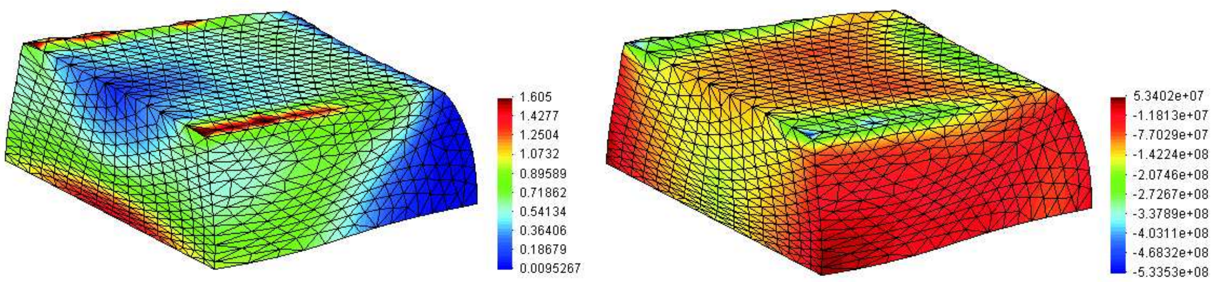

a) b)

Figure 13: Sidepressing of a cylinder, FIC algorithm ($a = 0.1$), tetrahedra, fine mesh (22186 elements): (a) effective plastic strain; (b) pressure distribution

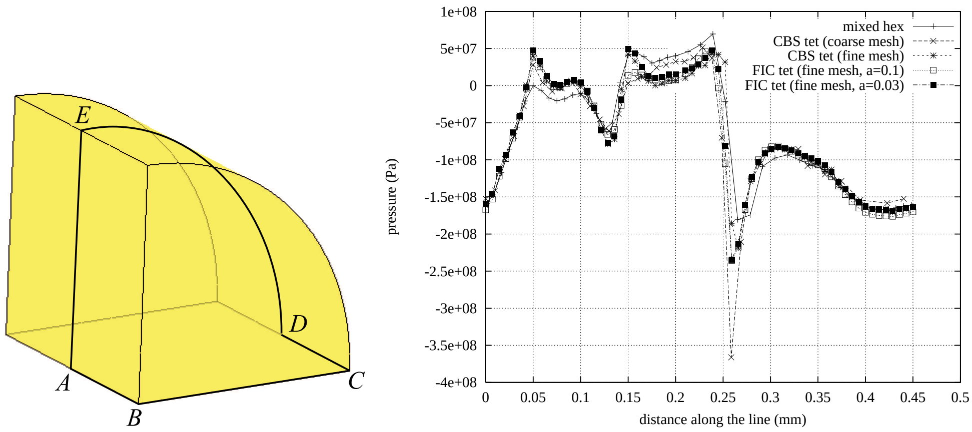

a) b)

Figure 14: a) Definition of the line for comparison of pressure distribution b) Pressure distribution along the line $ABCDEA$

6.3 Backward extrusion

Backward extrusion of a cylinder made of steel 16MNCr5 has been analysed. This is a benchmark example of the finite element program for forming simulation MARC/Autoforge [24]. The tooling and billet geometry are given in Fig. 15a. Initial material dimensions are the following: length 30 mm and diameter 30 mm. Punch of diameter 20 mm has a prescribed stroke of 28 mm. Material properties are as follows: Young's modulus $E = 3.24 \cdot 10^5$ MPa, Poissson's coefficient $\nu = 0.3$, material density $\rho = 8120$ kg/m^3, yield stress $\sigma_{Y0} = 300$ MPa and hardening modulus $H = 50$ MPa. Friction between the material and tools is defined by the Coulomb friction coefficient $\mu = 0.1$.

The simulation of the backward extrusion was carried out with remeshing employed to regenerate the meshes when element distorsion was excessive. Figures 15b and 15c show the results in the form of the final deformed shape with the distribution of the effective plastic strain obtained using quadrilaterals and mixed formulation, and using triangles and the CBS algorithm, respectively. The results are in a good agreement with the solution given in [24]. This example demonstrates use of the CBS algorithm in simulation of bulk forming processes.

7 Conclusions

The characteristic based split algorithm provides the necessary stabilization for linear triangles and tetrahedra. The extension of the CBS algorithm to solid mechanics is straightforward. Its implementation in the explicit dynamic finite element program allows the simulation of solid mechanics problems with quasi-incompressible deformation of materials typical for bulk metal forming problems, for instance. The results obtained using the CBS algorithm are in quite a good agreement with the results obtained using other methods: the mixed formulation with quadrialteral and hexahedral elements and the stabilized algorithm based on the finite calculus with triangular and tetrahedral elements.

Acknowledgments

The authors are thankful to Professor O.C. Zienkiewicz for inspiration, continuous encouragement and many useful discussions.

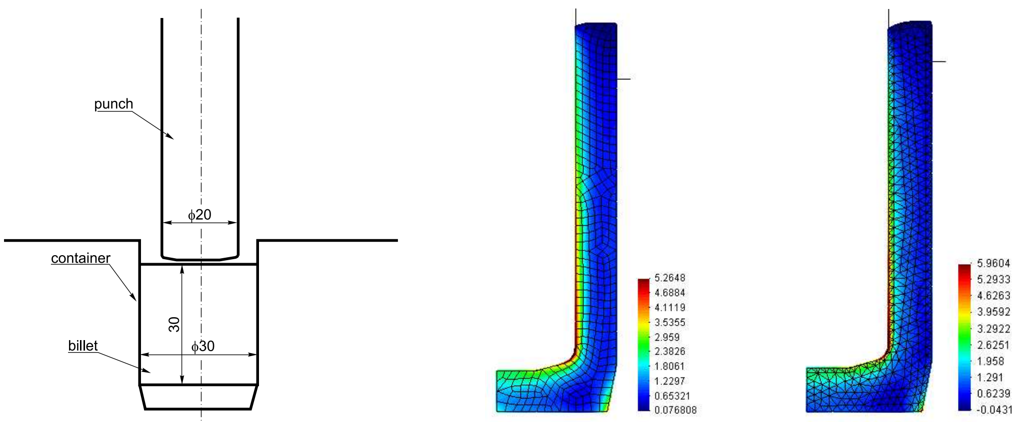

a) b)

Figure 15: Backward extrusion a) geometry definition, b) final deformed shape with effective plastic strain distribution, solution with quadrilaterals and mixed formulation, c) final deformed shape with effective plastic strain distribution, solution with triangles and the CBS algorithm

REFERENCES

[1] O.C. Zienkiewicz and R.L. Taylor. *The Finite Element Method*. Butterworth-Heinemann, Oxford, V edition, 2000.

[2] I. Babuška. The finite element method with lagrangian multipliers. *Numer. Math.*, 20:179–192, 1973.

[3] F. Brezzi. On the existence, uniqueness and approximation of saddle-point problems arising from Lagrange multipliers. *Rev. Française d'Automatique Inform. Rech. Opér., Ser. Rouge Anal. Numér.*, 8R-2:129–151, 1974.

[4] O.C. Zienkiewicz, S. Qu, R.L. Taylor, and S. Nakazawa. The patch test for mixed formulations. *Int. J. Num. Meth. Eng.*, 23:1873–1883, 1986.

[5] O.C. Zienkiewicz and R.L. Taylor. The finite element patch test revisited: A computer test for convergence, validation and error estimates. *Comput. Meth. Appl. Mech. Eng.*, 149:523–544, 1997.

[6] F. Brezzi and J. Pitkäranta. On the stabilization of finite element approximations of the Stokes problem. In W. Hackbusch, editor, *Efficient Solution of Elliptic Problems, Notes on Numerical Fluid Mechanics*. Vieweg, Wiesbaden, 1984.

[7] T.J.R. Hughes, L.P. Franca, and G.M. Hulbert. A new finite element formulation for computational fluid dynamics: VIII. The Galerkin/least-squares method for advective-diffusive equations. *Comput. Meth. Appl. Mech. Eng.*, 73:173–189, 1989.

[8] J. Bonet, H. Marriot, and O. Hassan. Stability and comparison of different linear tetrahedral formulations for nearly incompressible explicit dynamic applications. *Int. J. Num. Meth. Eng.*, 50:119–133, 2001.

[9] J. Bonet, H. Marriot, and O. Hassan. An average nodal deformation tetrahedron for large strain explicity dynamic applications. *Commun. Num. Meth. in Engrg.*, 17:551–561, 2001.

[10] R. Codina and J. Blasco. Stabilized finite element method for transient Navier-Stokes equations based on pressure gradient projection. *Comput. Meth. Appl. Mech. Eng.*, 182:287–300, 2000.

[11] R. Codina. Stabilization of incompressibility and convection through orthogonal subscales in finite element methods. *Comput. Meth. Appl. Mech. Eng.*, 190:1579–1599, 2000.

[12] M. Chiumenti, Q. Valverde, C. Agelet de Saracibar, and M. Cervera. A stabilized formulation for incompressible elasticity using linear displacement and pressure interpolations. *Comput. Meth. Appl. Mech. Eng.*, 2002.

[13] E. Oñate, R.L. Taylor, O.C. Zienkiewicz, and J. Rojek. A residual correction method based on finite calculus. *Eng. Comput.*, 20:629–658, 2003.

[14] A.J. Chorin. A numerical method for solving incompressible viscous problems. *Journal of Computational Physics*, 2:12–26, 1967.

[15] O.C. Zienkiewicz and R. Codina. A general algorithm for compressible and incompressible flow – Part I: The split, characteristic-based scheme. *Int. J. Num. Meth. Fluids.*, 20:869–885, 1995.

[16] O.C. Zienkiewicz, J. Rojek, R.L. Taylor, and M. Pastor. Triangles and tetrahedra in explicit dynamic codes for solids. *Int. J. Num. Meth. Eng.*, 43:565–583, 1998.

[17] J. Rojek, O.C. Zienkiewicz, E. Oñate, and E. Postek. Advances in FE explicit formulation for simulation of metalforming processes. *Journal of Materials Processing Technology*, 119(1-3):41–47, 2001.

[18] R. Codina. Pressure stability in fractional step finite element methods for incompressible flows. *Journal of Computational Physics*, 170:112–140, 2001.

[19] R. Rannacher. On Chorin's Projection Method for the Incompressible Navier-Stokes Equations. In J.G. Heywood, K. Masuda, R. Rautmann, and S.A. Solonnikov, editors, *The Navier–Stokes Equations II — Theory and Numerical Methods, Lecture Notes in Mathemathics, Proceedings of a Conference held Oberwolfach, Germany, 1991*, pages 167–183. Springer-Verlag, 1991.

[20] C. García Garino and J. Oliver. A numerical model for elastoplastic large strain problems. In D.R.J. Owen et al, editor, *Computational Plasticity*, 1992.

[21] E. Oñate. Derivation of stabilized equations for advective-diffusive transport and fluid flow problems. *Comput. Meth. Appl. Mech. Eng.*, 151:233–267, 1998.

[22] E. Oñate. A stabilized finite element method for incompressible flows using a finite increment calculus formulation. *Comput. Meth. Appl. Mech. Eng.*, 182:355–370, 2000.

[23] A. Brooks and T.J.R. Hughes. Streamline upwind/Petrov–Galerkin formulation for convection dominated flows with particular emphasis on the incompressible Navier–Stokes equations. *Comput. Meth. Appl. Mech. Eng.*, 32:199–259, 1982.

[24] *MARC/Autoforge User's Guide 2.2.* 1999.